Validity of the n^{-3} scaling law in dielectronic recombination processes

Jian-Guo Wang, Takako Kato, and Izumi Murakami
National Institute for Fusion Science, 322-6 Oroshi-cho, Toki-shi 509-5292, Japan
(Received 1 March 1999)

In the frame of quantum defect theory, a simplified relativistic configuration-interaction method is developed to study the dielectronic recombination (DR) processes. In this method, the infinite resonant doubly excited states involving high Rydberg states can be treated conveniently in a unified manner by interpolation. This provides an efficient method to check the validity of extrapolation based on the n^{-3} scaling law, which is widely used to treat the DR processes involving high Rydberg states. As an example, we studied the DR processes for Li-like argon, and the results are compared with the scaling laws and the experimental measurements, respectively. [S1050-2947(99)00809-4]

PACS number(s): 34.80.Kw, 34.80.Lx

I. INTRODUCTION

Dielectronic recombination (DR) can be regarded as a resonant radiative recombination process. As a free electron with a specific kinetic energy collides with an ion A^{q+}, one of the bound electrons of the ion A^{q+} is excited from the initial $n_i l_i$ orbital into the $n_f l_f$ orbital, the free electron is then captured into an unoccupied orbital nl and forms a resonant doubly excited state; subsequently, the resonant doubly excited state decays into a nonautoionizing state through radiative transition processes. Its importance in influencing the ionic balance in high-temperature plasmas, such as the solar corona, has been known for many years [1]. Its radiative emission is a significant contributor for plasma cooling in hot plasmas in fusion experiments. The dielectronic satellites of hydrogenlike ion have also been used to measure plasma densities in high density plasmas [2] and the electron temperatures in solar flares [3].

Many theoretical methods have been developed to calculate the DR process, such as the distorted-wave method [4,5], close coupling methods [6,7], nonrelativistic single configuration [8,9], and relativistic multiconfiguration methods [10,11]. In these calculations, it is tedious work to obtain the accurate DR rate coefficients since they involve many resonant doubly excited high Rydberg states. Due to the difficulty of numerical calculation on the wave function and the too enormous number of high Rydberg states, most calculations either neglect high-lying doubly excited states or simply use the n^{-3} scaling law to treat them [9,12–14]. Neglecting high-lying doubly excited states will induce inaccuracies in the DR calculations, especially for the low Z atom. The evaluation by the n^{-3} scaling law can give an improvement, but it should be checked for high Rydberg states. In order to check the validity of the n^{-3} scaling law, Karim and Bhalla have performed explicit DR calculations for Rydberg states ($n \leqslant 8$) on heliumlike ions using the Hartree-Fock atomic model [15], and found that the $1/n^3$ scaling law is appropriate when $n \geqslant 8$. However, this conclusion is not always correct for lower Z ions, we will discuss it in Sec. III.

In fact, quantum defect theory (QDT) has been developed to treat the atomic processes involving high Rydberg states [16–18], which was also used to study the DR cross sections and rate coefficients for high Rydberg states by extrapolation [7,19–21]. Recently, in the frame of QDT, we have developed a simplified relativistic configuration-interaction (SRCI) method to study the dielectronic recombination processes [22–24]. In this method, all the resonant doubly excited high Rydberg states are classified into different channels with same angular momentum quantum number and same angular momentum coupling type. In each channel, the defined energy-normalized matrix elements vary smoothly with the energy of high Rydberg states. Only a few points (including a continuum point) are calculated, the many resonant high Rydberg states can be treated in a unified manner by interpolation (rather than extrapolation), and then the DR cross sections and rate coefficients can be obtained conveniently. This method gives an overall description of all high Rydberg states in a channel, and avoids the inaccuracies of extrapolation through one point. By analyzing the energy-normalized matrix elements in a small energy domain, we can check the validity of the n^{-3} scaling law.

In this paper, as an example, we studied the DR processes of the $\Delta N = 0$ transition for Li-like argon. The DR processes have the form

$$e^- + \mathrm{Ar}^{15+}(1s^2 2s) \rightarrow \mathrm{Ar}^{14+}(1s^2 2pnl)^{**} \rightarrow \begin{cases} \mathrm{Ar}^{14+}(1s^2 2snl)^* + h\nu, \\ \mathrm{Ar}^{14+}(1s^2 2pn'l')^* + h\nu. \end{cases} \quad (1)$$

Due to energy conservation, the possible resonant doubly excited states appear at high Rydberg states ($n \geqslant 10$). It provides a good example to check the validity of the n^{-3} scaling law for high Rydberg states. The results on the SRCI method are compared with the scaling laws and the experimental measurements, respectively.

II. THEORETICAL METHOD

The cross section of resonant capture processes, in which the Ar^{15+} ion in initial state $i(1s^2 2s)$ captures a free electron with a specific energy ϵ_i and forms the Ar^{14+} ion in the resonant doubly excited state $j(1s^2 2pnl)$, can be treated in the isolated resonance approximation (atomic units are used throughout unless specified),

$$\sigma_{ij}^{c}=\frac{\pi^2\hbar^3}{m_e\epsilon_i}\frac{g_j}{2g_i}A_{ji}^{a}\ \delta(\epsilon-\epsilon_i), \tag{2}$$

where g_i and g_j are the statistical weight of the state i and j, respectively. A_{ji}^{a} is Auger decay rate (inverse resonant capture), which can be calculated by Fermi's golden rule,

$$A_{ji}^{a}=\frac{2\pi}{\hbar}\left|\left\langle \Psi_j\left|\sum_{s<t}\frac{1}{r_{s,t}}\right|\Psi_{i\epsilon_i}\right\rangle\right|^2, \tag{3}$$

where Ψ_j and $\Psi_{i\epsilon_i}$ are antisymmetrized many-electron wave functions for the j state and i state plus a free electron, respectively, and the continuum wave function of the free electron is energy normalized.

We construct the configuration wave functions $\phi(\Gamma JM)$ (Γ denotes the configuration $1s^22pnl$ and parity) as antisymmetrized product-type wave functions from central-field Dirac orbitals with appropriate angular momentum coupling [25]. All relativistic single-electron wave functions (bound and continuum) are calculated based on the atomic self-consistent potential obtained from the ground-state configuration for Ar^{14+} [26,27]. An atomic state function for the state $j(1s^22pnl)$ with total angular momentum JM is then expressed as a linear expansion of the configuration wave functions with the same principal quantum numbers $(2,n)$, and the same orbital angular momentum quantum numbers (p,l)

$$\psi_j(JM)=\sum_{\lambda=1}^{m}C_{j\lambda}\phi(\Gamma_\lambda JM). \tag{4}$$

Here m is the number of the configuration wave functions and the mixing coefficients $C_{j\lambda}$ for state j are obtained by diagonalizing the relevant Hamiltonian matrices [25]. The free state is chosen as the single configuration wave function. Then we have

$$A_{ji}^{a}=\frac{2\pi}{\hbar}\left|\sum_{\lambda=1}^{m}C_{j\lambda}M_{ij\lambda}^{a}\right|^2, \tag{5}$$

where the Auger decay matrix element $M_{ij\lambda}^{a}$ is defined as

$$M_{ij\lambda}^{a}=\left\langle \phi(\Gamma_\lambda JM)\left|\sum_{s<t}\frac{1}{r_{s,t}}\right|\Psi_{i\epsilon_i}\right\rangle. \tag{6}$$

Based on QDT, when l are fixed and n varies from bound to continuum state, all the resonant doubly excited states with the same J will form a channel. In the channel, the energy-normalized matrix element can be defined as

$$\overline{M}_{ij}^{a}=\sum_{\lambda=1}^{m}C_{j\lambda}M_{ij\lambda}^{a}(\nu_n^{3/2}/q). \tag{7}$$

Here (ν_n^3/q^2) is the density of state, $\nu_n=n-\mu_n$, μ_n is the corresponding quantum defect, and q equals the ionization degree of doubly excited states plus one. This energy-normalized matrix element $\overline{M}_{ij}^{a}$ varies smoothly with the electron orbital energy in the channel [22,24]. When the energy-normalized matrix elements of a few states (including one continuum state) in a channel have been calculated, the Auger decay matrix elements of infinite discrete states of that channel can be obtained by interpolation. From the expressions (7) and (5), the Auger rates and capture rates (by detailed balance) of the infinite resonant doubly excited states can be calculated conveniently.

The resonant doubly excited state may autoionize with a rate A_{ji}^{a} by reemitting Auger electron or decay radiately into a lower energy state k with a radiative rate A_{jk}^{r}, which is defined as

$$A_{jk}^{r}=\frac{4e^2\omega}{3\hbar c^3 g_j}|\langle\Psi_j|T^{(1)}|\Psi_k\rangle|^2, \tag{8}$$

where ω is photon energy and $T^{(1)}$ is electronic dipole operator [22]. The atomic wave function Ψ_k for final state k can be constructed in a way similar to the expression (4)

$$\psi_k(J'M')=\sum_{\lambda'=1}^{m'}C_{k\lambda'}\phi'(\Gamma'_\lambda J'M'). \tag{9}$$

Then we have

$$A_{jk}^{r}=\frac{4e^2\omega}{3\hbar c^3 g_j}\left|\sum_{\lambda,\lambda'=1}^{m,m'}C_{j\lambda}C_{k\lambda'}M_{\lambda,\lambda' jk}^{r}\right|^2, \tag{10}$$

where the radiative transition matrix element is defined as

$$M_{\lambda,\lambda' jk}^{r}=\langle\phi(\Gamma_\lambda JM)|T^{(1)}|\phi'(\Gamma'_\lambda J'M')\rangle. \tag{11}$$

For the radiative process with certain final state $k(1s^22snl)$ or $k(1s^22pn'l')$, the resonant doubly excited states with the fixed (l) and different orbital energy form a channel. In the channel, the energy-normalized radiative transition matrix element is defined as

$$\overline{M}_{jk}^{r}=\sum_{\lambda,\lambda'=1}^{m,m'}C_{j\lambda}C_{k\lambda'}M_{\lambda,\lambda' jk}^{r}(\nu_n^{3/2}/q). \tag{12}$$

This energy-normalized matrix element varies slowly with the electron orbital energy [22,29–31]. By interpolation, all the energy-normalized matrix elements of infinite discrete states in a channel can be obtained. From the expression (10), we can obtain all the radiative rates in the channel.

The resonance energy ϵ_i can be calculated under the frozen core approximation [32]. Then, we can obtain the DR cross sections for any resonant doubly excited states conveniently

$$\sigma_{ij;k}=\frac{\pi^2\hbar^3}{m_e\epsilon_i}\frac{g_j}{2g_i}P_{ij;k}\delta(\epsilon-\epsilon_i) \tag{13}$$

and

$$P_{ij;k}=\frac{A_{ji}^{a}A_{jk}^{r}}{\sum_{k'}A_{jk'}^{r}+\sum_{i'}A_{ji'}^{a}}. \tag{14}$$

Here the summation i' is over all possible states of Ar^{15+} ion, and the summation k' is over all possible states of Ar^{14+} whose energy are below state j.

The summation of cross sections over all possible k is expressed as

$$\sigma_{ij}=\sum_k \sigma_{ij;k}. \tag{15}$$

The DR strength S_{ij}, which is the integral of the DR cross section over the natural width of the resonance, can be written as

$$S_{ij}=\frac{\pi^2\hbar^3}{m_e\epsilon_j}\frac{g_j}{2g_i}\frac{A^a_{ji}\sum_k A^r_{jk}}{\sum_{k'} A^r_{jk'}+\sum_{i'} A^a_{ji'}}. \tag{16}$$

Using the velocity distribution of the free electron, we can obtain the dielectronic recombination rate coefficients.

III. RESULT AND DISCUSSION

There are enormous intermediate resonance states involved in the DR process, which makes the explicit calculations not practicable [15]. Hence, the n^{-3} scaling law is widely used in the literature to extrapolate the satellite intensity factors (proportional to DR cross section) for higher ($n \geqslant 4$) resonances [9,12–14]. Based on QDT, we have developed the SRCI method, in which all the high-lying resonant doubly excited states are treated conveniently through interpolation. This method provides an overall description on the behaviors of high Rydberg states, and can be regarded as an efficient method to check the validity of the n^{-3} scaling law. As an example, we studied the DR processes for Ar^{15+} ions, and calculated the Auger rates, radiative rates, integrated cross sections, and rate coefficients. In our calculation, we have included the doubly excited states $1s^22pnl$ with $10 \leqslant n \leqslant 15, l \leqslant 11$ (and corresponding continuum states) as benchmark points.

A. Auger rates

Using formulas (6) and (7), we can obtain the energy-normalized Auger transition matrix elements. As an example, we plotted the energy-normalized Auger transition matrix elements $\bar{M}^a_{ji}$ for four Auger channels in Fig. 1, which include $1s^22pns(^3P_0)\rightarrow 1s^22s+\varepsilon p_{1/2}$, $1s^22pnd(^3P_0)\rightarrow 1s^22s+\varepsilon p_{1/2}$, $1s^22png(^3F_2)\rightarrow 1s^22s+\varepsilon p_{3/2}$, $1s^22pnj(^3I_{11})\rightarrow 1s^22s+\varepsilon g_{9/2}$, and n changes from $n=10$ to $n=\infty$ and continuum states. In each channel, $\bar{M}^a_{ji}$ vary smoothly with the orbital energy of capture electron. There are infinitely many doubly excited high Rydberg states in a small energy domain below the threshold value. When the energy-normalized matrix elements of a few states (including one continuum state) in a channel have been calculated, all the Auger matrix elements of infinitely many doubly excited states of that channel can be obtained by interpolation. From the expressions (7) and (5), the Auger rates of the infinitely many resonant doubly excited states can be calculated conveniently. This method provides an overall description for high Rydberg states located in the small energy domain, which is not same as the method of widely used extrapolation by one points based on the n^{-3} scaling law.

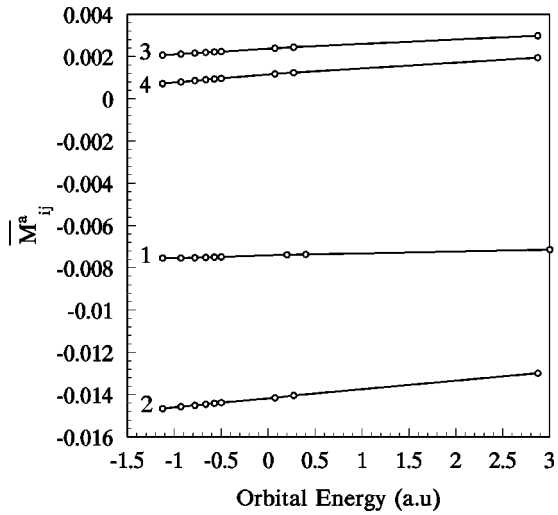

FIG. 1. Energy-normalized Auger matrix elements in four channels as a function of orbital energy. (1) $1s^22pns(^3P_0)\rightarrow 1s^22s+\varepsilon p_{1/2}$, (2) $1s^22pnd(^3P_0)\rightarrow 1s^22s+\varepsilon p_{1/2}$, (3) $1s^22png(^3F_2)\rightarrow 1s^22s+\varepsilon p_{3/2}$, (4) $1s^22pnj(^3I_{11})\rightarrow 1s^22s+\varepsilon g_{9/2}$. Circles are benchmark points, which are calculated explicitly (the circles in the following figures are the same).

In the calculation of Auger rates for high Rydberg doubly excited states, there are two ways to extrapolate the Auger rate based on the n^{-3} scaling law. One is extrapolation from the Auger rate of one Rydberg state with certain principal quantum number n_0 to these Rydberg states with higher principal quantum number n by $A^a_{ji}(n)=A^a_{ji}(n_0)\times n_0^3/n^3$ [33–35]. If we assume that our energy-normalized matrix elements are constant and the quantum defects can be neglected, namely, $\bar{M}^a_{ji}(n)=\bar{M}^a_{ji}(n_0)$ and $\mu_n=0$ when $n \geqslant n_0$, then we can obtain this scaling law from Eqs. (7) and (5). Another way is extrapolation from the threshold value of the according partial electron-impact excitation cross sections [36–38]. Our energy-normalized matrix elements above the threshold value are just the partial electron-impact excitation matrix elements with exchange. If we assume that our energy-normalized matrix elements below threshold value are constant and equal to the threshold value in a channel, and the quantum defects can be neglected, then from Eqs. (7) and (5), we can obtain the n^{-3} scaling law in Refs. [36–38].

From the above analysis, we can conclude that if the n^{-3} scaling law is well preserved, it is necessary that the energy-normalized matrix elements below threshold value are almost constant in the small energy domain where high Rydberg states are located. So we can check the validity of the n^{-3} scaling law in these two extrapolations by analyzing whether the energy-normalized matrix elements in the small energy domain below the threshold value are constant in a channel. In our example, the energy-normalized matrix elements near the threshold value are almost constant in most of the channels, as shown in Fig. 1. This means that the n^{-3} scaling law should be well preserved for these channels. However, it can be seen that as the orbital quantum number l increases, the changing of the energy-normalized matrix elements in the small domain becomes large, so it can be expected that the deviation from the n^{-3} scaling law also becomes large with increasing l. This can be confirmed from

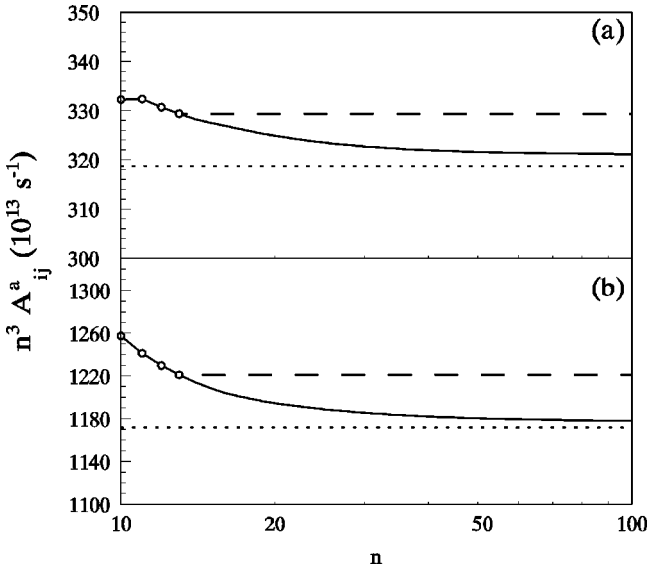

FIG. 2. Auger rates multiplied by n^3 in two channels as a function of n. Solid line: interpolation on SRCI method; dashed line: extrapolation from $n_0=13$; dotted line: extrapolation from threshold value. (a) $1s^22pns(^3P_0)\rightarrow 1s^22s+\varepsilon p_{1/2}$, (b) $1s^22pnd(^3P_0)\rightarrow 1s^22s+\varepsilon p_{1/2}$.

the Auger rates in Figs. 2 and 3, which are corresponding to the four channels in Fig. 1.

For $1s^22pns(^3P_0)\rightarrow 1s^22s+\varepsilon p_{1/2}$ and $1s^22pnd(^3P_0)\rightarrow 1s^22s+\varepsilon p_{1/2}$ channels, because the curve of energy-normalized matrix elements is almost constant as the curves 1 and 2 shown in Fig. 1, the results from interpolation on SRCI method and two extrapolation on n^{-3} scaling law are in agreement within a few percent as shown in Fig. 2. For $1s^22png(^3F_2)\rightarrow 1s^22s+\varepsilon p_{3/2}$ channel, the difference of SRCI method and two extrapolation methods is within 15% as shown in Fig. 3(a). For the $1s^22pnj(^3I_5)\rightarrow 1s^22s+\varepsilon i_{11/2}$ channel, the difference approaches 100% as shown in Fig. 3(b), this is because the relative variation of $\overline{M^a}$ is large with increasing l, as shown in Fig. 1. The fundamental reason is as following: for a smaller values of radial distance r, the energy-normalized wave functions vary slowly with orbital energy [18,28], which implies the scaling law for the Auger or radiative rate [28]. But this cannot be extended to bigger r. So the states with a relatively big amplitude of wave function in smaller r have good scaling law. As l increases, the effect of the centrifugal term becomes strong, which cause a relatively big amplitude of the wave function in bigger r. So the accuracy of the n^{-3} scaling law becomes low with increasing l, as shown in Figs. 2 and 3. As n increases, the difference increases between interpolation on the SRCI method and the first type of extrapolation and decreases between interpolation and the second type of extrapolation, as shown in Fig. 3. This comes from the different initial points for the extrapolation.

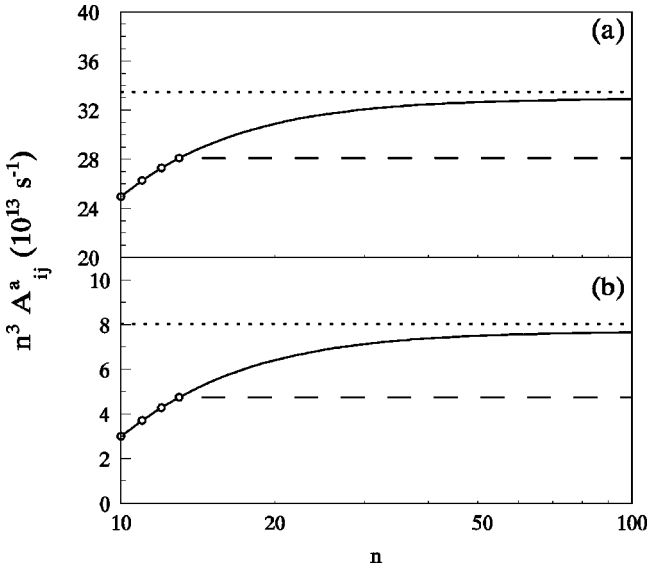

FIG. 3. Auger rates multiplied by n^3 in two channels as a function of n. Solid line, interpolation on SRCI method; dashed line, extrapolation from $n_0=13$; dotted line, extrapolation from threshold value. (a) $1s^22png(^3F_2)\rightarrow 1s^22s+\varepsilon p_{3/2}$; (b) $1s^22pnj(^3I_{11})\rightarrow 1s^22s+\varepsilon g_{9/2}$.

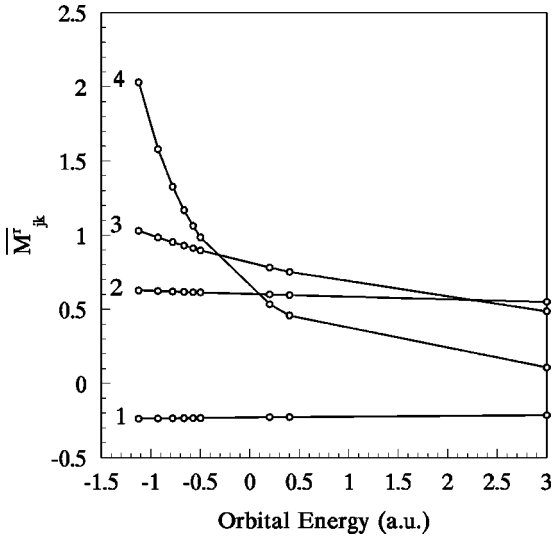

FIG. 4. Energy-normalized radiative transition matrix elements in four channels as a function of orbital energy. (1) $1s^22pns(^3P_0)\rightarrow 1s^22p^2(^3P_1)$, (2) $1s^22pnd(^3P_0)\rightarrow 1s^22p^2(^3P_1)$, (3) $1s^22png(^3F_2)\rightarrow 1s^22p4f(^3D_1)$, (4) $1s^22pnj(^3I_5)\rightarrow 1s^22p7i(^3H_4)$.

B. Radiative rates

Here, we only consider two main types of dipole transition processes, as shown in formula (1). For $Ar^{14+}(1s^22pnl)^{**}\rightarrow Ar^{14+}(1s^22snl)^{*}+h\nu$ (rate is denoted as A^r_{1jk}), the radiative rates are almost unchanged with n in a channel. We calculated explicitly the rates of states with $n\leqslant n_0$. For the states with $n>n_0$, we approximate $A^r_{1jk}(n)=A^r_{1jk}(n_0)$. For $Ar^{14+}(1s^22pnl)^{**}\rightarrow Ar^{14+}(1s^22pn'l')^{*}+h\nu$ (the rate is denoted as A^r_{2jk}), we can calculate the energy-normalized radiative transition matrix elements using Eqs. (13) and (14). This energy-normalized matrix element varies smoothly with the orbital energy of captured electron [22,29–31]. By interpolation, all the energy-normalized matrix elements of infinitely many doubly excited states in a channel can be obtained. From expressions (12) and (10), we can obtain all the radiative rates in the channel. In Fig. 4, the energy-normalized radia-

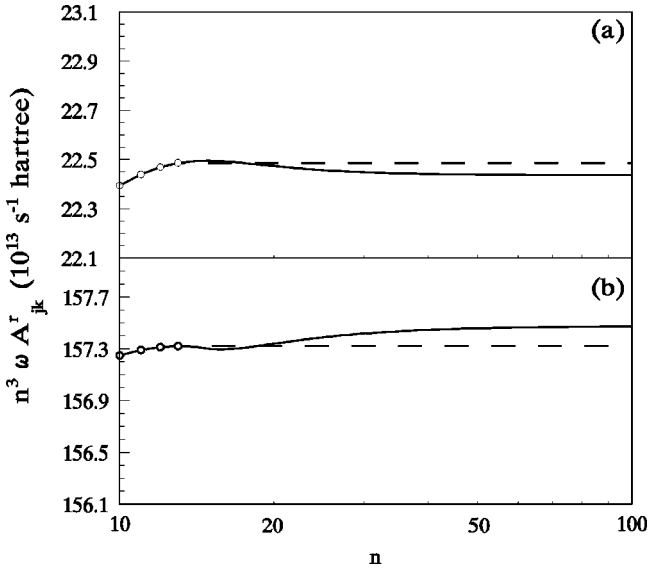

FIG. 5. Radiative transition rates multiplied by n^3 in two channels as a function of n. Solid line, interpolation on SRCI method; dashed line, extrapolation from $n_0=13$. (a) $1s^22pns(^3P_0)\rightarrow 1s^22p^2(^3P_1)$; (b) $1s^22pnd(^3P_0)\rightarrow 1s^22p^2(^3P_1)$.

tive matrix elements in four channels are plotted, which include $1s^22pns(^3P_0)\rightarrow 1s^22p^2(^3P_1)$, $1s^22pnd(^3P_0)\rightarrow 1s^22p^2(^3P_1)$, $1s^22png(^3F_2)\rightarrow 1s^22p4f(^3D_1)$, $1s^22pnj(^3I_5)\rightarrow 1s^22p7i(^3H_4)$, and n changes from $n=10$ to $n=\infty$ and continuum states. Each curve varies smoothly with the orbital energy, and all the transition processes involving infinitely many high Rydberg states are located in a small energy domain below the threshold value, which can be treated conveniently by interpolation. The radiative rates according to these channels are plotted in Figs. 5 and 6. If we assume that our radiative energy-normalized matrix elements are constant and quantum defects can be neglected for high

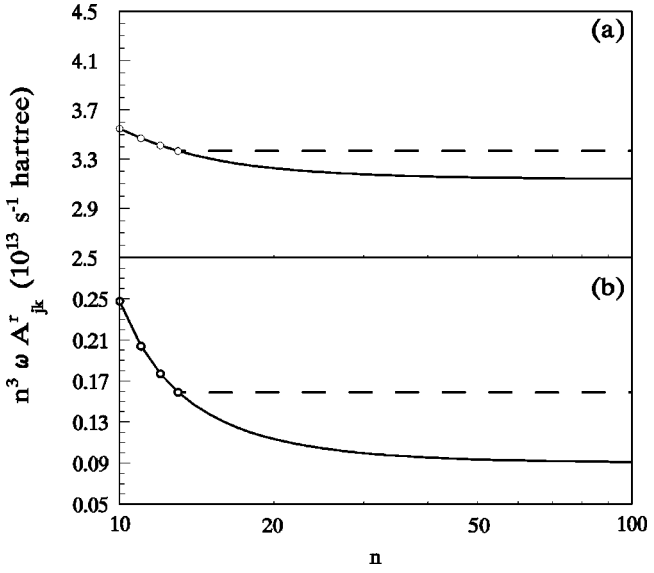

FIG. 6. Radiative transition rates multiplied by n^3 in two channels as a function on n. Solid line, interpolation on SRCI method; dashed line, extrapolation from $n_0=13$. (a) $1s^22png(^3F_2)\rightarrow 1s^22p4f(^3D_1)$; (b) $1s^22pnj(^3I_5)\rightarrow 1s^22p7i(^3H_4)$.

Rydberg states, namely, $\bar{M}^r_{jk}(n)=\bar{M}^r_{ji}(n_0)$ and $\mu_n=0$ when $n\geqslant n_0$, we can derive the n^{-3} scaling law $A^r_{2jk}(n)=A^r_{2jk}(n_0)\times(n_0^3\omega_0)/(n^3\omega)$ [33–35]; here ω is the energy of emitting photon. By analyzing whether the radiative energy-normalized matrix elements $\bar{M}^r_{jk}$ below the threshold value are constant, we can check the validity of the n^{-3} scaling law in a channel.

For $1s^22pns(^3P_0)\rightarrow 1s^22p^2(^3P_1)$ and $1s^22pnd(^3P_0)\rightarrow 1s^22p^2(^3P_1)$ channels, $\bar{M}^r_{jk}$ are almost unchanged in the small energy domain below the threshold value as the curves 1 and 2 shown in Fig. 4, so n^{-3} scaling law can be well preserved within 1% as shown in Fig. 5. However, as angular momentum quantum l increases, the variation of $\bar{M}^r_{jk}$ becomes large in the small energy domain, as shown in Fig. 4, and the differences between SRCI method and extrapolating method also become large. For $1s^22png(^3F_2)\rightarrow 1s^22p4f(^3D_1)$ channel, the difference is about 10% as shown in Fig. 6(a), and for $1s^22pnj(^3I_5)\rightarrow 1s^22p7i(^3H_4)$, the difference approaches 80%.

It should be noted that for a certain initial state, the energy-normalized transition matrix element may have nodes, at which the matrix element is equal to zero [39]. In this case, the interpolation should be carried out for the energy-normalized transition elements but not for the radiative rates (i.e., proportional to the square of the transition elements); of course, the n^{-3} scaling law cannot be used in this case.

C. Integrated cross sections

In some works [40,35], the DR integrated cross sections or rate coefficients have been extrapolated to high Rydberg states directly by the n^{-3} scaling law. Because the DR integrated cross sections or rate coefficients are proportional to $P_{ij,k}$ in Eq. (13), this extrapolation is equivalent to extrapolating the $P_{ij,k}$ and is also equivalent to extrapolating the dielectronic satellite factors [9,12–14].

This extrapolation can only be applied to two cases. One is $A^a_{ji}\ll\Sigma_k A^r_{jk}$; then we have $A^a_{ji}\Sigma_k A^r_{jk}/(\Sigma_{k'}A^r_{jk'}+\Sigma_{i'}A^a_{ji'})\simeq A^a_{ji}$ and the n^{-3} scaling law can be used, which often appears in the DR processes for middle or high Z ions. Another is $A^a_{ji}\gg\Sigma_k A^r_{jk}$ and $\Sigma_k A^r_{1jk}\ll\Sigma_k A^r_{2jk}$; then we have $A^a_{ji}\Sigma_k A^r_{jk}/(\Sigma_{k'}A^r_{jk'}+\Sigma_{i'}A^a_{ji'})\simeq\Sigma_k A^r_{2jk}$ and the n^{-3} scaling law can be used. For low Z ions, $A^a_{ji}\gg\Sigma_k A^r_{jk}$ and $A^r_{1jk}\gg\Sigma_k A^r_{2jk}$, then we have $A^a_{ji}\Sigma_k A^r_{jk}/(\Sigma_{k'}A^r_{jk'}+\Sigma_{i'}A^a_{ji'})\simeq\Sigma_k A^r_{1jk}\simeq$const, so the n^{-3} scaling law cannot be used in DR processes for low Z ions [22,41], and Karim and Bhalla's conclusion [15] cannot be extended to lower Z ions ($Z<10$). For our example, the comparisons of A^a_{ji}, $\Sigma_k A^r_{1jk}$, $\Sigma_k A^r_{2jk}$ and $\Sigma_k A^r_{1jk}+\Sigma_k A^r_{2jk}$ in four channels are shown in Figs. 7 and 8. As n increases, A^a_{ji} and $\Sigma_k A^r_{2jk}$ (the second type of radiative process) decrease, but $\Sigma_k A^r_{1jk}$ (the first type of radiative process) is almost unchanged. For lower n, $A^a_{ji}\gg\Sigma_k A^r_{1jk}+\Sigma_k A^r_{2jk}$ and $\Sigma_k A^r_{2jk}\gg\Sigma_k A^r_{1jk}$, as shown in Figs. 7 and 8. However, for higher n, $\Sigma_k A^r_{1jk}\gg\Sigma_k A^r_{2jk}$, and even for higher l, $\Sigma_k A^r_{1jk}+\Sigma_k A^r_{2jk}\gg A^a_{ji}$, as shown in Fig. 8, the conditions to extrapolate directly $P_{ij;k}$ cannot be satisfied.

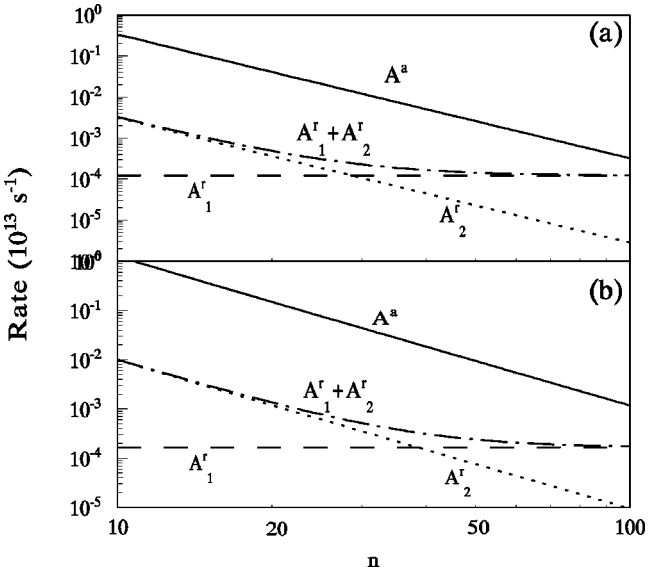

FIG. 7. Auger and radiative rates in two channels as a function of n. Solid line, Auger rates; dashed line, radiative transition rates for $Ar^{14+}(1s^22pnl)^{**}\rightarrow Ar^{14+}(1s^22snl)^{*}+h\nu$; dotted line, radiative transition rates for $Ar^{14+}(1s^22pnl)^{**}\rightarrow Ar^{14+}(1s^22pn'l')^{*}+h\nu$; dash-dotted line, sum of above radiative transition rates. (a) $1s^22pns(^3P_0)$ channel; (b) $1s^22pnd(^3P_0)$ channel.

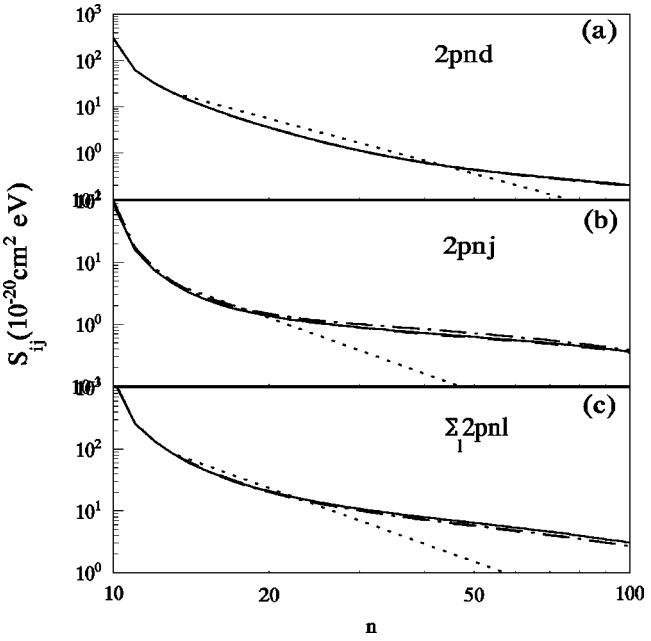

FIG. 9. Integrated cross sections for different doubly excited states as a function of n. Solid line, interpolation on SRCI method; dashed line, extrapolation of $A^a(n=13)$ and $A^r(n=13)$; dash-dotted line, extrapolation of A^a (threshold value) and $A^r(n=13)$; dash-dotted line, extrapolation of $P_{ij;k}$. (a) $1s^22pns$; (b) $1s^22pnj$, (c) sum of $1s^22pnl(l=1,2,\ldots,11)$.

The integrated cross sections S_{ij} in Eq. (16) for doubly excited states $1s^22pnd$, $1s^22pnj$, and the sum of $1s^22pnl(l=1,2,\ldots,11)$ are shown in Fig. 9. We compare our results from the SRCI method with that from three extrapolations on the n^{-3} scaling law, including (1) A^a_{ji} and A^r_{jk} are extrapolated from $n_0=13$, (2) A^a_{ji} is extrapolated from the threshold value and A^r_{ji} is extrapolated from $n_0=13$, (3) $P_{ij;k}$ is extrapolated from $n_0=13$. For $1s^22pnd$ resonances, the results from the first and second extrapolations are in good agreement with those from our SRCI method, as shown in Fig. 9(a), but the third extrapolation cannot give an agreement, because the condition for the third extrapolation has not been satisfied, as we have discussed. With the increasing l of $1s^22pnl$ resonances, the differences among the first and second extrapolations and SRCI method become relatively large, as shown in Fig. 9(b). However, the main contributions to integrated cross sections come from the resonances with relatively small l, so the differences for total integrated cross sections are small among the first and second extrapolations and SRCI method, as shown in Fig. 9(c). The above results show that the errors and variations in the calculations of the individual transition probabilities may be large, such as in Figs. 3 and 5, but because the DR integrated cross sections are proportional to the $P_{ij,k}$, the errors and variations tend to cancel in the evaluation of the integrated cross sections [40,42], and we can still obtain good agreements among the SRCI method and the first and second extrapolation. But if we extrapolate the $P_{ij,k}$, the errors in $P_{ij,k}$ will affect the cross sections and rate coefficients directly, so we must check the condition before extrapolating $P_{ij,k}$.

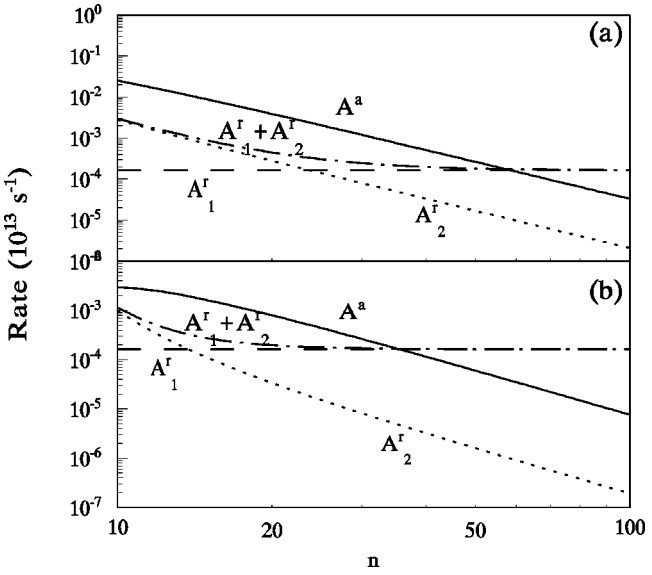

FIG. 8. Auger and radiative rates in two channels as a function of n. Solid line, Auger rates; dashed line, radiative transition rates for $Ar^{14+}(1s^22pnl)^{**}\rightarrow Ar^{14+}(1s^22snl)^{*}+h\nu$; dotted line, radiative transition rates for $Ar^{14+}(1s^22pnl)^{**}\rightarrow Ar^{14+}(1s^22pn'l')^{*}+h\nu$; dash-dotted line, sum of above radiative transition rates. (a) $1s^22png(^3F_2)$ channel; (b) $1s^22pnj(^3I_5)$ channel.

The contributions of $1s^22pnl$ resonances with different n and different l are shown in Fig. 10. As n increases, the relative contributions of the resonances with high l increase. There are two main reasons. First, for high-n resonances, $Ar^{14+}(1s^22pnl)^{**}\rightarrow Ar^{14+}(1s^22snl)^{*}+h\nu$ dominates the radiative processes, which is almost nondependent on l, as shown in Figs. 7 and 8. Second, the statistical weight g_j in Eq. (13) increases with l, which partly cancels the decreasing of A^a_{ji}. These make S_{ij} decrease slowly with l. Gener-

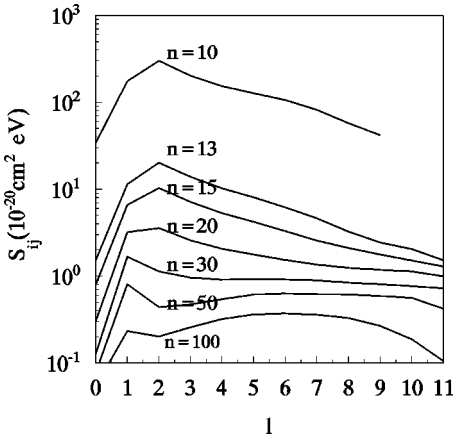

FIG. 10. Integrated cross sections with different n for resonances $1s^2 2pnl$ as a function of l.

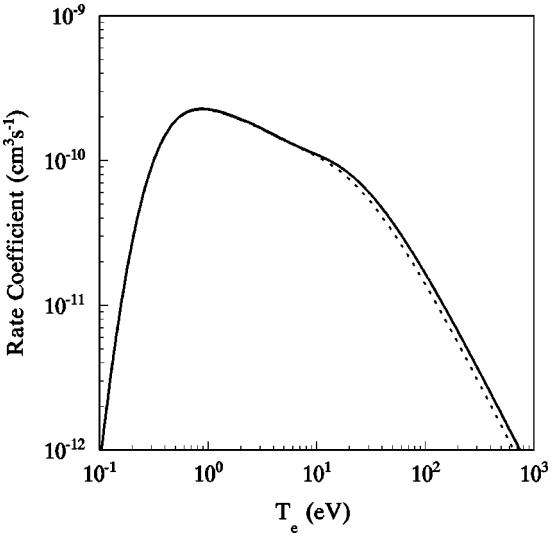

FIG. 12. Maxwellian average rate coefficients as a function of temperature. Solid line: interpolation on SRCI method; dashed line: extrapolation of $A^a(n=13)$ and $A^r(n=13)$; dash-dotted line: extrapolation of A^a (threshold value) and $A^r(n=13)$; dotted line: extrapolation of $P_{ij;k}$.

ally, the integrated cross section S_{ij} in Eq. (13) is a function of A^a_{ji}, A^r_{jk}, and g_j, which have a different dependence on n and l, so when we analyze the integrated cross sections S_{ij} in Fig. 10, we must consider their synthetical effects.

D. Rate coefficients

We calculated the rate coefficients for the DR processes of the $\Delta N=0$ transition for Li-like argon. Figure 11(a) shows the theoretical rate coefficients, which are obtained from integrated cross sections folded with the electron beam temperatures (20 meV/k_B transverse temperature and 0.13 meV/k_B longitudinal temperature) [43]. Figure 11(b) shows the Zong *et al.* experimental measurements [44,45], where a background of 5×10^{-9} cm^3 s^{-1} has been subtracted. The theoretical and experimental line positions compare rather well. In the spectra one can identify Rydberg states up to $n=18$ for the $1s^2 2p_{1/2}$ core excitation and $n=25$ for the $1s^2 2p_{3/2}$ core excitation, as shown in Fig. 11, where we only give labels for a few resonances for simplicity. In general, the theoretical rate coefficients are a little smaller than experimental measurements for high Rydberg states. The possible reasons include: the background is not fully substracted, the contribution of high $l(l\geqslant12)$ resonances is ignored, and an external field may also have a visible influence on it [46]. We will discuss these effects further in a future work.

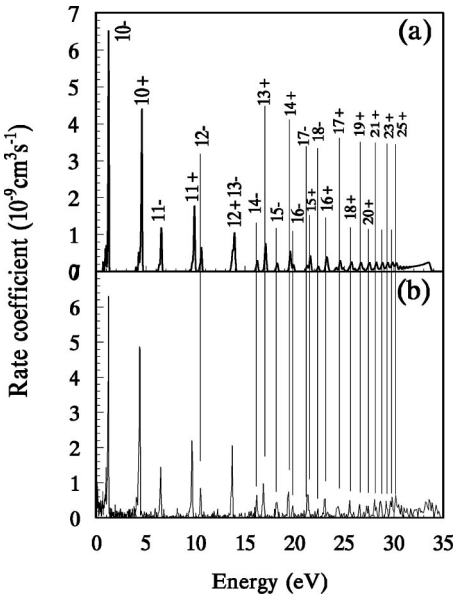

FIG. 11. DR rate coefficients as a function of relative energy. $-$: $1s^2 2p_{1/2}$ core excitation; $+$: $1s^2 2p_{3/2}$ core excitation. (a) Theoretical results on SRCI method (folded with 20 meV/k_B transverse temperature and 0.13 meV/k_B longitudinal temperature), (b) Experimental measurements [44] (a background of 5×10^{-9} cm^3 s^{-1} has been subtracted).

The total Maxwellian average rate coefficients for the $\Delta N=0$ transition are shown in Fig. 12. The respective extrapolations of Auger and radiative rates on n^{-3} scaling laws can give a good agreement with the SRCI calculation, within 2%, which cannot be distinguished from SRCI results in Fig. 12. The extrapolating of $P_{ij;k}$ gives a difference of between 10 and 20 % when $T_e\geqslant20$ eV, as show in Fig. 12. Because the contribution of high-l resonances is a small part and the errors of the individual transition probabilities tend to cancel [40,42], the large differences in high-l resonances (as shown in Figs. 3 and 6) are not very important in the total rate coefficients.

IV. CONCLUSION

In this paper, a simplified relativistic configuration interaction method is used to study the dielectronic recombination processes. In this method, the infinite resonant doubly excited states involving a high Rydberg state can be treated conveniently in a unified manner by interpolation. This method gives an overall description of all high Rydberg states in a channel, and avoids the inaccuracies of extrapolation through one point. By analyzing the energy-normalized matrix elements in a small energy domain, we can check the

validity of the extrapolating method based on the widely used n^{-3} scaling laws. In the DR calculation from Li-like to Be-like argon, we found that the respective extrapolations of Auger and radiative rates on n^{-3} scaling laws can give good results for DR cross sections and rate coefficients, although the difference between the extrapolation and SRCI method increases with increasing l in $1s^2 2pnl$ resonances. However, when we extrapolate $P_{ij;k}$, we must consider the valid condition; otherwise, the errors may be very large. Due to the fully relativistic treatments, our SRCI method can be used to study the DR processes for any Z elements with any electrons. We will continue to check the validity of scaling laws for other systems in the future.

ACKNOWLEDGMENTS

The authors would like to thank Dr. W. Zong for providing us with their experimental data and Professor Fujimoto for his helpful discussions. This work was supported by the Japan Society for Promotion of Science.

[1] A. Burgess, Astrophys. J. **139**, 776 (1964).
[2] A. V. Vinogradov, I. Yu. Skobelev, and E. A. Yukov, Zh. Eksp. Teor. Fiz. **72**, 1762 (1977) [Sov. Phys. JETP **45**, 925 (1977)].
[3] J. Dubau, A. H. Gabriel, M. Loulergue, L. Steenman-Clark, and S. Volone, Mon. Not. R. Astron. Soc. **195**, 705 (1981).
[4] W. Eissner and M. J. Seaton, J. Phys. B **6**, 2187 (1972).
[5] D. R. Flower and J. M. Launay, J. Phys. B **5**, L207 (1972).
[6] H. E. Saraph and M. J. Seaton, Philos. Trans. R. Soc. London, Ser. A **271**, 1 (1971).
[7] J. Dubau, Ph.D. thesis, University of London, 1973.
[8] Y. Hahn, Phys. Rev. A **22**, 2896 (1980).
[9] D. J. McLaughlin and Y. Hahn, Phys. Rev. A **29**, 712 (1984).
[10] M. H. Chen, Phys. Rev. A **31**, 1449 (1985).
[11] H. P. Saha, Phys. Rev. A **49**, 894 (1994).
[12] E.g., M. H. Chen, Phys. Rev. A **33**, 994 (1986); J. Dubau, A. H. Gabriel, M. Loulergue, L. Steennan-Clark, and S. Volonte, Mon. Not. R. Astron. Soc. **195**, 705 (1981).
[13] K. R. Karim and C. P. Bhalla, Phys. Rev. A **37**, 2599 (1988).
[14] J. Nilson, J. Quant. Spectrosc. Radiat. Transf. **36**, 539 (1986).
[15] K. R. Karim and C. P. Bhalla, Phys. Rev. A **43**, 615 (1991).
[16] M. Gailtis, Zh. Eksp. Teor. Fiz. **44**, 1974 (1963) [Sov. Phys. JETP **17**, 1328 (1963)].
[17] U. Fano, J. Opt. Soc. Am. **65**, 979 (1975).
[18] M. J. Seaton, Proc. Phys. Soc. London **88**, 801 (1966); Rep. Prog. Phys. **46**, 167 (1983).
[19] M. J. Seaton and P. J. Storey, in *Atomic Processes and Applications*, edited by P. G. Burke and B. L. Moiseiwitsch (North-Holland, Amsterdam, 1976), p. 133.
[20] J. Dubau and S. Volonte, Rep. Prog. Phys. **43**, 167 (1980).
[21] R. H. Bell and M. J. Seaton, J. Phys. B **18**, 1589 (1985).
[22] Jian-Guo Wang, Yi-Zhi Qu, and Jia-Ming Li, Phys. Rev. A **52**, 4274 (1995).
[23] Jian-Guo Wang, Yu Zou, Chen-Zhong Dong, and Jia-Ming Li, Chin. Phys. Lett. **12**, 530 (1995).
[24] Chen-Zhong Dong, Yu Zou, Jian-Guo Wang, and Jia-Ming Li, Acta Phys. Sin. **44**, 1712 (1995).
[25] Zhong-Xin Zhao and Jia-Ming Li, Acta Phys. Sin. **34**, 1469 (1985).
[26] Jia-Ming Li and Zhong-Xing Zhao, Acta Phys. Sin. **31**, 97 (1982).
[27] D. A. Liberman, D. T. Cromer, and J. T. Waber, Comput. Phys. Commun. **2**, 107 (1971).
[28] R. D. Cowan, *The Theory of Atomic Structure and Spectra* (University of California Press, Berkeley, 1981), p. 227.
[29] Lei Liu and Jia-Ming Li, Acta Phys. Sin. **42**, 1901 (1993).
[30] Jian-Guo Wang, Xiao-Ming Tong, and Jia-Ming Li, Acta Phys. Sin. **45**, 13 (1996); see also Yi-Zhi Qu, Jian-Guo Wang, and Jia-Ming Li, *ibid.* **46**, 249 (1997).
[31] Cheng Zhu, Jian-Guo Wang, Yi-Zhi Qu, and Jia-Ming Li, Phys. Rev. A **57**, 1747 (1998).
[32] C. M. Lee and Jia-Ming Li, Phys. Rev. A **10**, 584 (1974).
[33] K. Moribayashi and T. Kato (unpublished).
[34] K. Moribayashi and T. Kato, Phys. Scr. **55**, 286 (1997).
[35] A. Peleg, E. Behar, P. Mandelbaum, and J. L. Schwob, Phys. Rev. A **57**, 3493 (1998).
[36] M. J. Seaton, Mon. Not. R. Astron. Soc. **119**, 81 (1959).
[37] T. Fujimoto, T. Kato, and Y. Nakamura (unpublished).
[38] C. J. Romanik, Astrophys. J. **330**, 1022 (1988).
[39] E.g., X. L. Liang and J. M. Li, Acta Phys. Sin. **34**, 1479 (1985); M. S. Wang and R. H. Pratt, Phys. Rev. A **29**, 174 (1984); **35**, 1154 (1987); X. M. Tong, L. Yang, and J. M. Li, Acta Phys. Sin. **38**, 407 (1989).
[40] Y. Hahn, Adv. At. Mol. Phys. **21**, 123 (1985).
[41] Yi-Zhi Qu, Jian-Guo Wang, Jian-Kui Yuan, and Jia-Ming Li, Phys. Rev. A **57**, 1033 (1998).
[42] Y. Hahn, Rep. Prog. Phys. **60**, 691 (1997).
[43] G. Kilgus, D. Habs, D. Schwalm, A. Wolf, N. R. Badnell, and A. Muller, Phys. Rev. A **46**, 5730 (1992).
[44] W. Zong, R. Schuch, E. Lindroth, H. Gao, D. R. DeWitt, S. Asp, and H. Danared, Phys. Rev. A **56**, 386 (1997).
[45] R. Schuch, D. R. DeWitt, H. Gao, S. Mannervik, W. Zong, and N. R. Basnell, Phys. Scr. **73**, 114 (1997).
[46] S. Schennach, A. Muller, O. Uwira, J. Haselbauer, W. Spies, A. Frank, M. Wagner, R. Becker, M. Kleinod, E. Jennewein, N. Angert, P. H. Mokler, N. R. Badnell, and M. S. Pindzola, Z. Phys. D **30**, 291 (1994).